# Numerical study on the Eulerian-Lagrangian analysis of Navier-Stokes turbulence

K. Ohkitani

*Department of Applied Mathematics,*

*School of Mathematics and Statistics,*

*The University of Sheffield, Hicks Building,*

*Hounsfield Road Sheffield S3 7RH, U.K.*

P. Constantin

*Department of Mathematics,*

*The University of Chicago*

*Chicago, Il 60637, USA*

(Dated: February 12, 2008)

## Abstract

Detailed analyses of the Navier-Stokes equations on the basis of the Euler-Lagrangian formalism are presented with use of numerical simulations. A singular perturbation property arising in the limit of vanishing viscosity is one issue of this paper. By using the connection matrix, which is related with the geometry of particle paths, we introduce "connection anomaly" for the characterization of the property and confirm it numerically. As a characterization in physical space, we show how regions with small values of a determinant of a derivative of diffusive labels are spatially correlated with vortex structures.

Two kinds of initial conditions are examined; (i) decaying isotropic turbulence developing from a random initial condition and (ii) the orthogonally offset two vortex tubes. For (i), it is found that when turbulence is fully-developed, the resetting process occurs very frequently, which defines a short time scale associated with small-scale motion. For (ii), we confirm our previous finding that resetting of diffusive label captures successfully reconnection of vortex at higher Reynolds numbers. Even for this special initial condition, turbulence is developed after the phase of prominent reconnection and frequent resettings are associated with it.

# I. INTRODUCTION

One of the important properties of the the Navier-Stokes flows is that in the limit of vanishing viscosity their behavior differ from that of corresponding Euler equations which are known to possess a number of inviscid invariants. For example, in the inviscid case the total kinetic energy is conserved, where as in slightly viscous Navier-Stokes flows it is observed that the energy is dissipated at a nontrivial rate at finite time. This anomalous behavior, finite energy dissipation in the limit of small viscosity is the fundamental premise of Kolmogorov similarity in the theory of turbulence. As another example, it is well known that the vortex lines are frozen in inviscid fluids, where as vortex reconnection can (and indeed do) occur in slightly viscous fluids.

There are some previous researches regarding the difference between inviscid and viscous fluid motion. For example, it was proved that a Navier-Stokes flow converges to the corresponding Euler flow in the limit of vanishing viscosity as long as the latter flows remains smooth [1].

Recently, a framework of the Navier-Stokes equations that is suitable for studying theoretically and numerically topological properties of vortex lines in viscous flow has been developed by one of the authors [2–4]. It has been applied to numerical simulations of the Navier-Stokes equations and its usefulness for monitoring vortex reconnection has been established [5]. This may be regarded as the first practical use of Weber transform in viscous fluids. See also an interesting generalization recently made in [6]. We will discuss some natural questions arising out of the previous work including: is it useful to characterize fully-developed turbulence ? In particular, is it possible to detect also an anomalous behavior on the basis of this formalism ?

This Eulerian-Lagrangian framework is based on a generalization of Weber's transform (see Eqs.(4),(5) below) to a viscous fluid. It incorporates nonlocal interaction and viscous diffusion in a multiplicative fashion. The formalism has been developed for the mathematical theory of Navier-Stokes equations [2–4]. Nevertheless, with purely analytical methods it is difficult to analyze long time evolution of the Navier-Stokes equations under which vortex reconnection actually takes place.

We present here results of Eulerian-Lagrangian analyses using numerical simulations of the Navier-Stokes equations. In a previous work it was found that this formalism captures

vortex reconnection successfully, in the sense that frequent resetting take place when vortices undergo reconnection.

The question we raise here is to see how this Eulerian-Lagrangian formalism characterize fully-developed turbulence. Two cases of initial conditions will be considered; (i) Random initial condition and (ii) orthogonally off-set vortex tubes. In (i), we mainly discuss 'connection anomaly' (to be introduced below), which is an alternative characterization of singular perturbative nature of developed turbulence in the Eulerian-Lagrangian formalism. Case (ii) is a higher Reynolds number version of experiments reported before by ourselves. Estimates of virtual velocity, derivative of $\boldsymbol{A}$ and their $\nu$-dependence are discussed, together with the physical meaning of $\mathrm{Det}(\nabla \boldsymbol{A}) = 0$. We will show that the connection is particularly suited both for characterization of vortex reconnection and for singular perturbation property of the inviscid limit of the fluid equations.

The mathematical formulation will be described In Section II and the numerical methods in Section III. Section IV is the main part of this paper, where decaying turbulence is analyzed in some details with the Eulerian-Lagrangian formalism. In Section V, some analyses will be presented regarding experiments on vortex reconnection at higher Reynolds numbers. Finally, Section VI will be devoted to summary and outlook.

## II.  THE EULERIAN-LAGRANGIAN FORMULATION

With standard notation, the Navier-Stokes equations and the continuity equation read

$$\frac{\partial \boldsymbol{u}}{\partial t} + (\boldsymbol{u} \cdot \nabla)\boldsymbol{u} = -\nabla p + \nu \triangle \boldsymbol{u}, \tag{1}$$

and

$$\mathrm{div}\ \boldsymbol{u} = 0, \tag{2}$$

where $\boldsymbol{u}$ stands for velocity, $p$ for pressure and $\nu$ for kinematic viscosity. Using another dependent variable called impulse $\boldsymbol{w}$, which is not incompressible in general, we may alternatively describe time evolution of the flow by the following equations

$$\frac{\partial \boldsymbol{w}}{\partial t} + (\boldsymbol{u} \cdot \nabla)\boldsymbol{w} = -(\nabla \boldsymbol{u})^T \boldsymbol{w} + \nu \triangle \boldsymbol{w}, \tag{3}$$

where $T$ denotes a matrix transpose. The usual incompressible velocity $\boldsymbol{u}$ is obtained by solenoidal projection $\boldsymbol{P}$ of $\boldsymbol{w}$

$$\boldsymbol{u} = \boldsymbol{P}(\boldsymbol{w}). \tag{4}$$

3

This formalism is sometimes referred to as the impulse formalism, see *e.g.* [22]. There are many references regarding the impulse formalism and its related issues. See, for example, [7–26].

It should be noted that $\boldsymbol{w}$ can be represented in a multiplicative fashion as follows

$$\boldsymbol{w} = (\nabla \boldsymbol{A})^T \boldsymbol{v}. \tag{5}$$

In this decomposition, $\boldsymbol{A}$ denotes the diffusive Lagrangian label and $\boldsymbol{v}$ the virtual velocity, that is, it is assumed to obey the following equations [2]

$$\frac{\partial \boldsymbol{A}}{\partial t} + (\boldsymbol{u} \cdot \nabla)\boldsymbol{A} = \nu \triangle \boldsymbol{A}. \tag{6}$$

In order to be consistent with the Navier-Stokes equations, we find that $\boldsymbol{v}$ should obey

$$\frac{\partial \boldsymbol{v}}{\partial t} + (\boldsymbol{u} \cdot \nabla)\boldsymbol{v} = 2\nu \boldsymbol{C} : \nabla \boldsymbol{v} + \nu \triangle \boldsymbol{v}, \tag{7}$$

where the $i-$th component of $\boldsymbol{C} : \nabla \boldsymbol{v}$ is given by $C_{m,k;i}\dfrac{\partial v_m}{\partial x_k}$ and

$$C_{m,k;i} = \frac{\partial x_j}{\partial A_i} \frac{\partial^2 A_m}{\partial x_j \partial x_k}.$$

The connection tensor allows a number of different interpretations. First, it is a coefficient in the viscous diffusion term in the equation for virtual velocity. Second, it has differential geometric meaning as a metric which relates $\boldsymbol{x}$ with $\boldsymbol{a}$ spaces. Third, it measures non-commutativity between Eulerian and Eulerian-Lagrangian derivatives. It is important to bear in mind that $\boldsymbol{C}$ measures non-commutativity between the Euler and Euler-Lagrange derivatives as indicated in the commutation relation $[\nabla_A^i, \nabla_E^k] = C_{m,k;i}\nabla_A^m$. On top of

$$\boldsymbol{\omega}(\boldsymbol{x}, t) = \nabla \times \boldsymbol{u}(\boldsymbol{x}, t)$$

we define virtual vorticity by

$$\boldsymbol{\zeta}(\boldsymbol{x}, t) = \nabla_A \times \boldsymbol{v}(\boldsymbol{x}, t).$$

A set of Equations (4,5,6,7) forms a closed system which is equivalent to the Navier-Stokes equations. We note that 'derivatives' with respect to $\boldsymbol{A}$, which is a dependent variable, are defined using $(\nabla \boldsymbol{A})^{-1}$ and chain rule, see [2–4] for details.

Cauchy formula generalized to viscous fluids reads

$$\boldsymbol{\omega} = \mathrm{Det}(\nabla \boldsymbol{A})(\nabla \boldsymbol{A})^{-1}\boldsymbol{\zeta}. \tag{8}$$

The determinant of gradient of diffusive labels is not conserved, but it changes as

$$\left(\frac{\partial}{\partial t} + \boldsymbol{u} \cdot \nabla\right) \mathrm{Det}(\nabla\boldsymbol{A}) = \nu \mathrm{Det}(\nabla\boldsymbol{A})\left(C_{i,k,;j}C_{j,k;i} + \partial_i C_{j,i,;j}\right), \tag{9}$$

or

$$\left(\frac{\partial}{\partial t} + \boldsymbol{u} \cdot \nabla - \nu\triangle\right) \log(\mathrm{Det}(\nabla\boldsymbol{A})) = \nu C_{i,k,;j}C_{j,k;i}. \tag{10}$$

We also note that

$$\frac{\partial}{\partial x_i}\mathrm{Det}(\nabla\boldsymbol{A}) = C_{j,i,;j}. \tag{11}$$

The choice of the variables $\boldsymbol{A}$ and $\boldsymbol{v}$ may not be unique. For example, if we take

$$\frac{\partial\boldsymbol{A}}{\partial t} + (\boldsymbol{u} \cdot \nabla)\boldsymbol{A} = 0,$$

as in the standard definition of Lagrangian markers, then we have

$$\frac{\partial\boldsymbol{v}}{\partial t} + (\boldsymbol{u} \cdot \nabla)\boldsymbol{v} = \nu\left((\nabla\boldsymbol{A})^T\right)^{-1}\triangle\left((\nabla\boldsymbol{A})^T\boldsymbol{v}\right)$$

However, this equation has third-order derivatives of $\boldsymbol{A}$, but the equation for $\boldsymbol{A}$ has no regularizing factor for it, and hence unbalanced. It may not be useful in practice.

## III.   NUMERICAL METHOD

Two technical points of the numerical method that should be mentioned are as follows. As a basic equation, we have rewritten (3) as

$$\frac{\partial\boldsymbol{w}}{\partial t} = -\nabla(\boldsymbol{w} \cdot \boldsymbol{u}) + \boldsymbol{u} \times \boldsymbol{\omega} + \nu\triangle\boldsymbol{w}, \tag{12}$$

because fast Fourier transforms can be implemented efficiently this way [29]. Another aspect is that it is not straightforward to evolve $\boldsymbol{v}$ because $\boldsymbol{C}$, a cubic quantity in $\boldsymbol{A}$, is cumbersome to handle. Instead of dealing with $\boldsymbol{v}$ directly, we have solved for displacement vector $\boldsymbol{\ell} = \boldsymbol{A} - \boldsymbol{x}$, which satisfies a set of passive equations

$$\frac{\partial\boldsymbol{\ell}}{\partial t} + (\boldsymbol{u} \cdot \nabla)\boldsymbol{\ell} = -\boldsymbol{u} + \nu\triangle\boldsymbol{\ell}. \tag{13}$$

In practice, we have solve a system of equations (12) and (13) simultaneously. Once $\boldsymbol{\ell}$ is known we can compute $\nabla\boldsymbol{A}$ by

$$\frac{\partial A_i}{\partial x_j} = \frac{\partial l_i}{\partial x_j} + \delta_{ij},$$

and the connection coefficients $\boldsymbol{C}$ and all other quantities of interest can be obtained *a posteori* by matrix inversion.

In inviscid fluids the determinant of $\nabla\boldsymbol{A}$ is unchanged and its invertibility, that is, $\boldsymbol{x}$ as a function of $\boldsymbol{a}$, is maintained automatically under the time evolution of the Euler equations. In the case of viscous fluids the determinant is not preserved in general [2]. Therefore, it is possible that it becomes zero and the matrix can become non-invertible under the time evolution of the Navier-Stokes equations. Indeed, according to our previous report [5], this actually takes place. In order to ensure the invertibility it is necessary to reset $\boldsymbol{\ell} = 0$ when the determinant becomes very small. Practically, we reset

$$\boldsymbol{\ell} = 0 \text{ if } \min_{\boldsymbol{x}} \mathrm{Det}(\nabla\boldsymbol{A}) \leq \epsilon,$$

where $\epsilon$ is a preassigned small parameter. Since the equation for $\boldsymbol{\ell}$ is passive, the resetting procedure does not affect the evolution of $\boldsymbol{u}$. Also, it has been shown that qualitative properties regarding the resetting frequency of $\boldsymbol{\ell}$ are independent of $\epsilon$ (See [4]).

The number of FFTs needed for simulating the incompressible Navier-Stokes equations using the vorticity formalism is 9 at each stage of Runge-Kutta scheme. The number is 13 if the impulse formalism (which deals with compressible variables) is used. If the displacement is simultaneously computed the number is 25, with additional 9 FFTs for the evaluation of the Jacobian determinant.

A $2/3-$dealiased pseudo-spectral method was employed under periodic boundary conditions. The number of grid points used were $128^3$, $256^3$ and $512^3$. Time marching was performed with a standard fourth-order Runge-Kutta scheme.

It turned out that for an accurate calculation of $\boldsymbol{C}$ we need to make the Reynolds number lower than commonly adopted to ensure the accuracy of velocity and vorticity. More precisely, it turned out that $k_{\max}/k_d \geq 1.4$ may be sufficient for resolving $\boldsymbol{\omega}$, but not for $\boldsymbol{C}$. In the calculations presented here we have $k_{\max}/k_d \geq 2$ which ensures accuracy of both $\boldsymbol{\omega}$ and $\boldsymbol{C}$. Here $k_{\max}$ is the maximum wavenumber and $k_d$ is the Kolmogorov dissipative wavenumber.
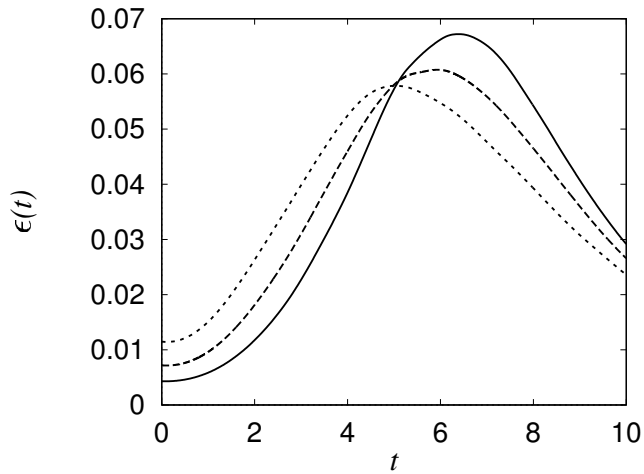
FIG. 1: Time evoultion of the energy disspation rate with $\nu = 1.5 \times 10^{-3}$(solid), $2.5 \times 10^{-3}$(dashed), $4 \times 10^{-3}$(dotted).

## IV.   DECAYING TURBULENCE

### A.   General properties

Before discussing the Eulerian-Lagrangian analyses we check that the turbulent flows we will consider have standard properties.

The initial condition has an energy spectrum of the form

$$E(k) = ck^2 \exp(-k^2),$$

where the constant $c$ is chosen in such a way that

$$\langle |\boldsymbol{u}|^2 \rangle = 1.$$

Numerical parameters used are summarized in Table I.

In Fig.1 we show time development of the dissipation rate of energy for three different Reynolds numbers. For the higher Reynolds number case, the total energy becomes shows a noticeable decay around $t = 4$ followed by a peak of its dissipation rate around $t = 6$.

In Fig.2 it is shown that $R_\lambda$ is around 100 or smaller after $t = 6$ and the product $\eta k_{\max}$ is greater than 1.3, showing that the flow field is well resolved throughout the computations. The situation is even better for the lower Reynolds number case. However, as we will see below the connection tensor $\boldsymbol{C}$ is a little bit under-resolved for the case with the

7
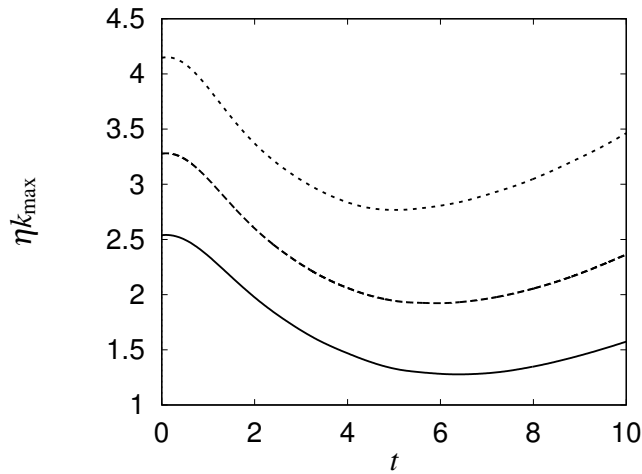
FIG. 2: Time evoultion of the $\eta k_{\mathrm{d}}$, plotted with the same line convention as in Fig.1.

highest Reynolds number. Therefore for the analysis of $\boldsymbol{C}$, we will use the results with the intermediate Reynolds number.

In Fig.3 the spectra of energy is shown at several different times, in which a short inertial subrange consistent with Kolmogorov similarity law $E(k) \propto k^{-5/3}$ at $t = 6$. Also, the tail of the spectra at large wavenumbers shows an exponential decay, consistent with well-resolved numerical solutions.

We introduce a (squared) norm of $\boldsymbol{\ell}$ as

$$E_{\boldsymbol{\ell}}(t) = \frac{1}{2} \left\langle |\boldsymbol{\ell}|^2 \right\rangle$$

and a (squared) norm of $\nabla \times \boldsymbol{\ell}$ as

$$Q_{\boldsymbol{\ell}}(t) = \frac{1}{2} \left\langle |\nabla \times \boldsymbol{\ell}|^2 \right\rangle,$$

where

$$\langle \ \rangle \equiv \frac{1}{(2\pi)^3} \int d\boldsymbol{x}.$$

We show their development in Fig.4, 6, 5 for different values of $\nu$.

The first resetting takes place at $t = 1.59$, independent of $\nu$. It is of interest to note that it is almost the same for three different values of viscosity despite the fact viscosity is necessary for a resetting to take place. This is on the order of, but smaller than, a large-scale eddy turn-over times $T$ defined by

$$T = \frac{2\pi}{\sqrt{\langle |\boldsymbol{u}|^2 \rangle}} \approx 6.28.$$

8
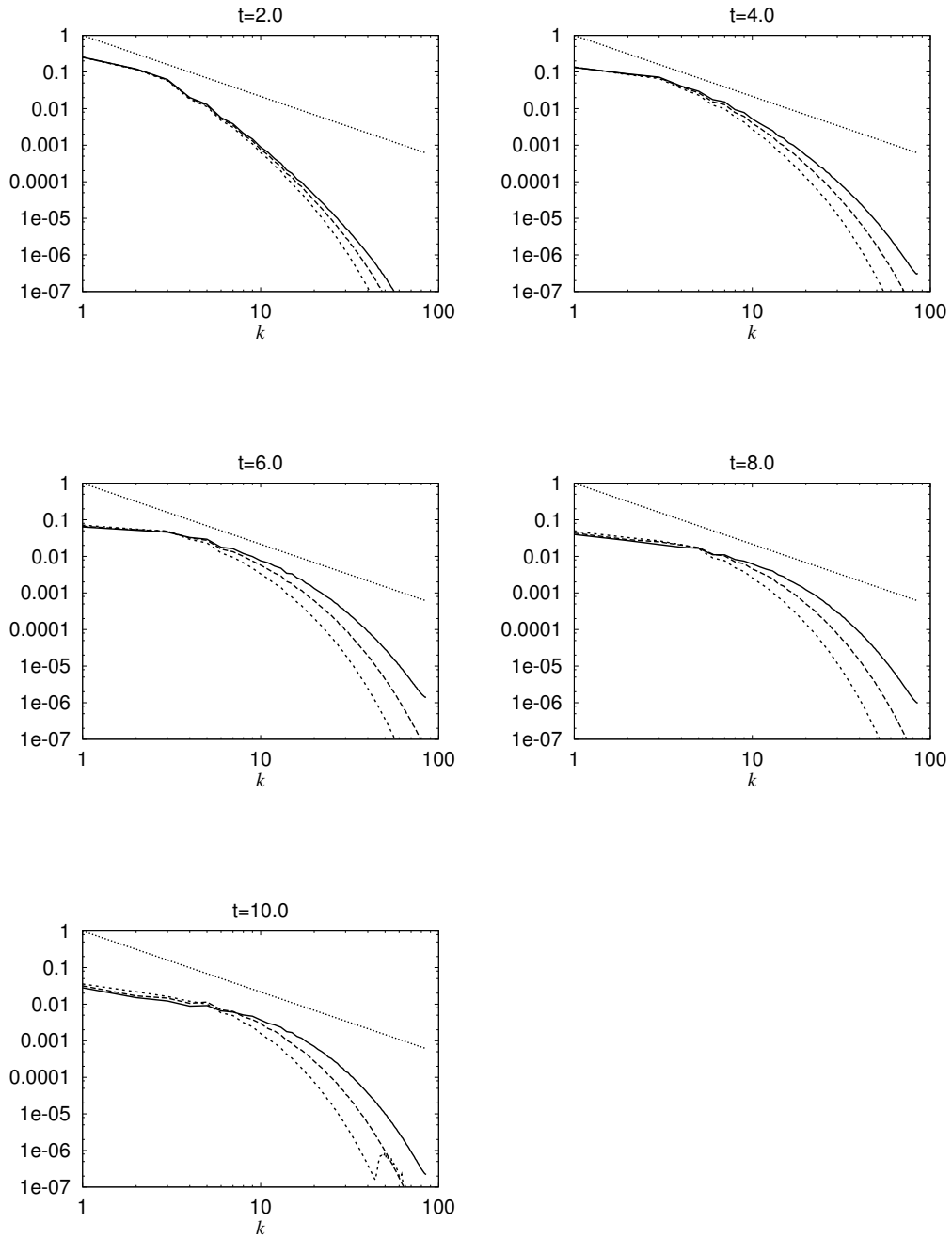
FIG. 3: Time evoultion of energy sepctra, plotted with the same line convention as in Fig.1.

The resetting time interval $\Delta t_j$ defined by

$$\Delta t_j = t_j - t_{j-1}, \text{ for } j = 1, 2, ...,$$

where $t_0 = 0$ and $t_j$ is the time of $j-$th resetting. In the early stage, the resetting time interval becomes shorter and shorter and it saturates around the time of maximum enstrophy ($t = 4$). Then it starts to increase slowly.

9
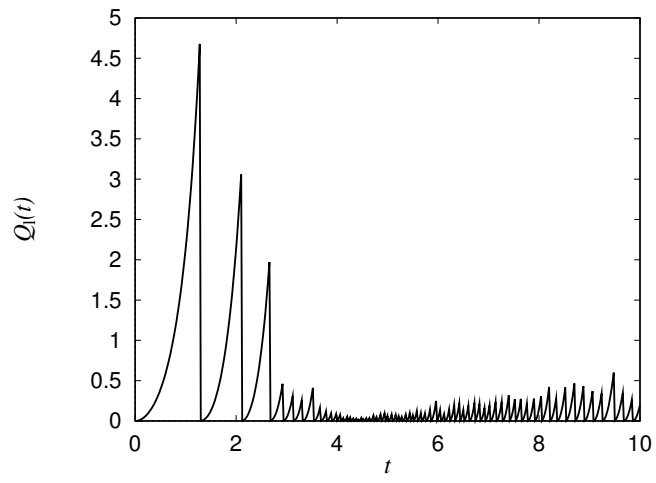
FIG. 4: Time evoultion of a (squared) norm $Q_l(t)$ of curl of displacement for $\nu = 1.5 \times 10^{-3}$.
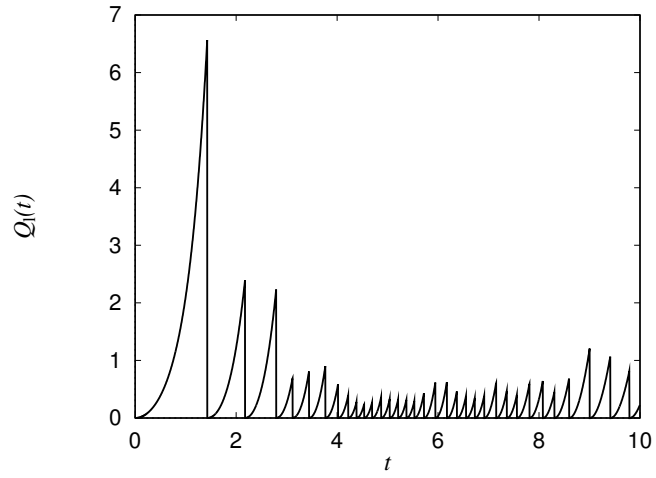


FIG. 5: Time evoultion of $Q_l(t)$ for $\nu = 2.5 \times 10^{-3}$.
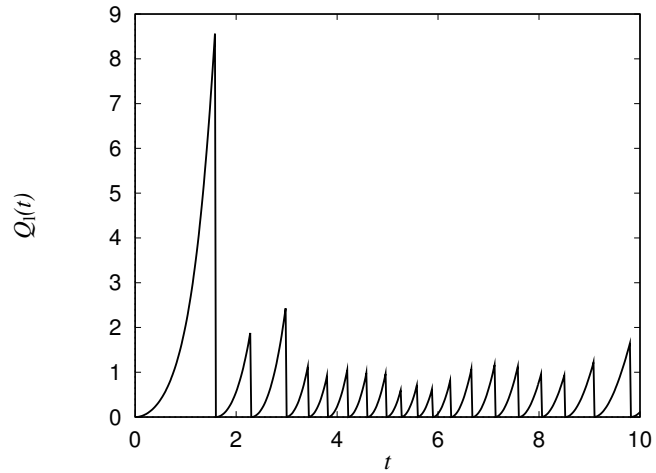


FIG. 6: Time evoultion of $Q_l(t)$ for $\nu = 4 \times 10^{-3}$.

10
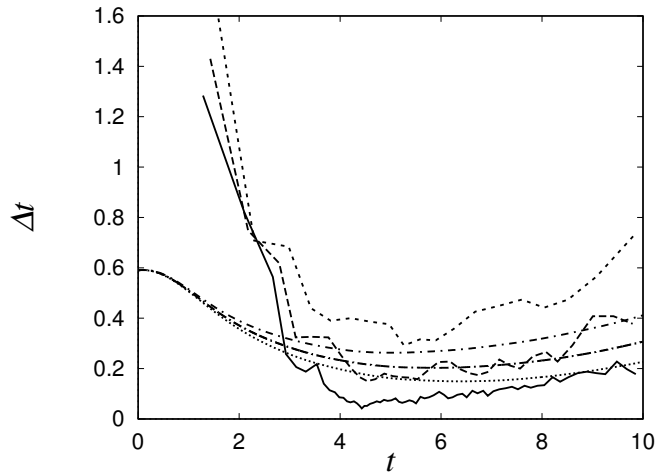
FIG. 7: Resetting time intervals $\Delta t$ for $\nu = 1.5 \times 10^{-3}$(solid), $2.5 \times 10^{-3}$(dashed), and $4.0 \times 10^{-3}$(short-dashed). Also, shown is the Komogorov time scale $\tau_K$ for $\nu = 1.5 \times 10^{-3}$(dotted), $2.5 \times 10^{-3}$(dash-dotted), $4 \times 10^{-3}$(short-dash-dotted).

In Fig.7 we compare the resetting time $\Delta t$ with the Kolmogorov time scale $\tau_{\mathrm{K}}$

$$\tau_{\mathrm{K}} = \sqrt{\frac{\nu}{\epsilon_{\mathrm{dis}}}}.$$

For each Reynolds number (particularly, the two larger ones), the resetting time interval is on the same order of Kolmogorov time scale.

In the inviscid case $\nu = 0$ no resetting can take place, because of volume preservation $\mathrm{Det}(\nabla \boldsymbol{A}) = 1$. If the RHS of (7) is negligible in the limit of small viscosity, then $\boldsymbol{v}$ is constant.

While the frequent resettings allow an interpretation as manifestation of vortex reconnection, the first resetting is known only to be on the order of a large-scale turn-over times. This time scale is the one by which excitation reach large wave numbers where the viscous effects are no longer negligible. The present result indicates that the determinant hits zero as soon as the viscous effects are important.

## B. The connection tensor

We recall some basic properties of the connection matrix. Connection $\boldsymbol{C}$ has a number of different meanings: it is a prefactor in front of a dissipative term in the equation for virtual velocity, and it is closely related to differential geometry of transformation $\boldsymbol{A}(\boldsymbol{x})$, and finally

11
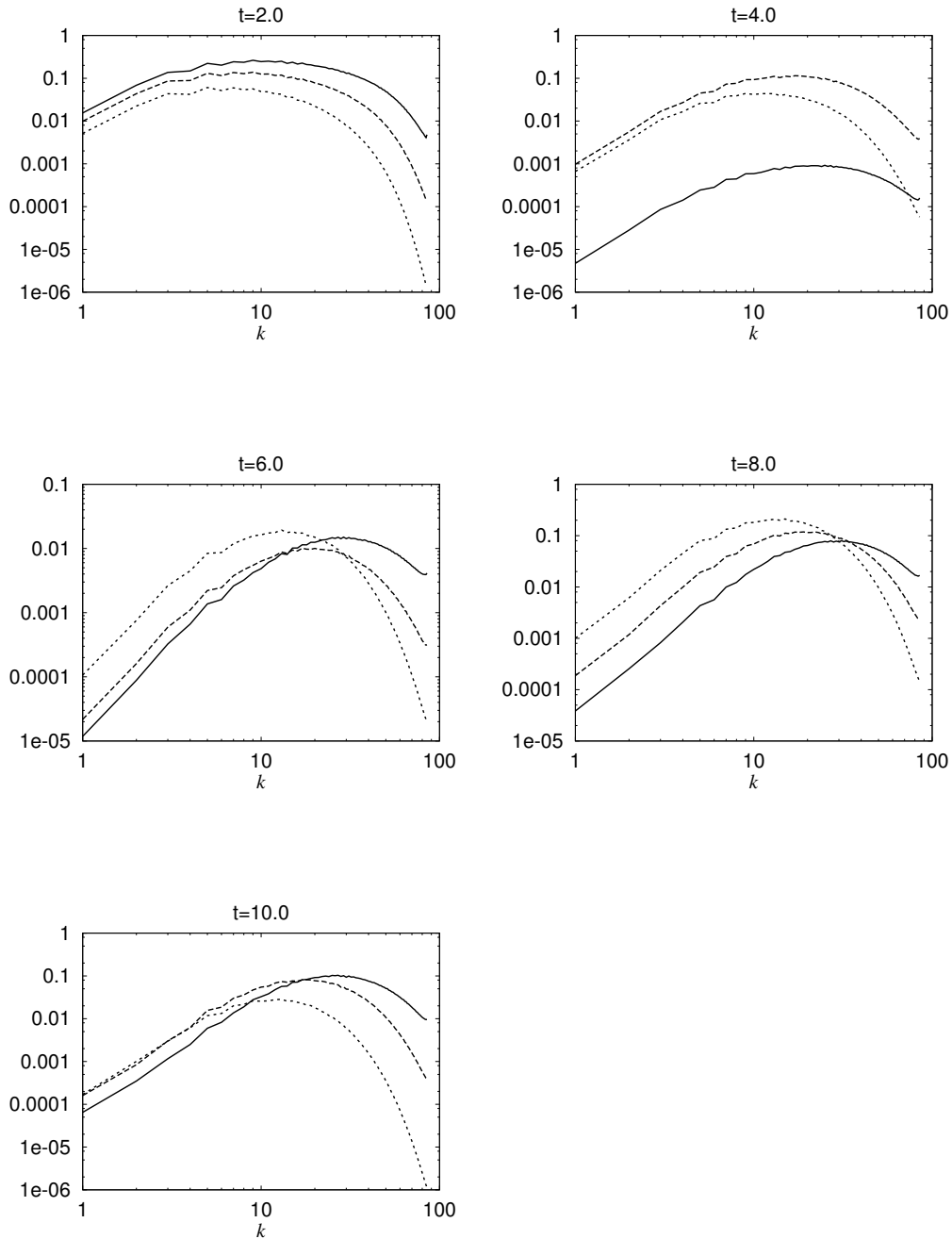
FIG. 8: Time evolution of spectra of connection, plotted with the same line convention as in Fig.1.

it measures non-commutativity between Eulerian- abd $\boldsymbol{A}$-derivatives.

In Fig.8 we show the Fourier spectrum of $\boldsymbol{C}$ averaged over its 27 components

$$E_{\boldsymbol{C}}(k) = \frac{1}{2} \sum_{i,j,k=1}^{3} \frac{1}{27} |\tilde{C(\boldsymbol{k})}_{i,j;k}|^2,$$

where $\tilde{C}_{i,j;k}(\boldsymbol{k})$ is the Fourier transform of $C_{i,j;k}(\boldsymbol{x})$. Their magnitude is not important because of their linear dynamics and because of resetting. Their shape at high wavenumber
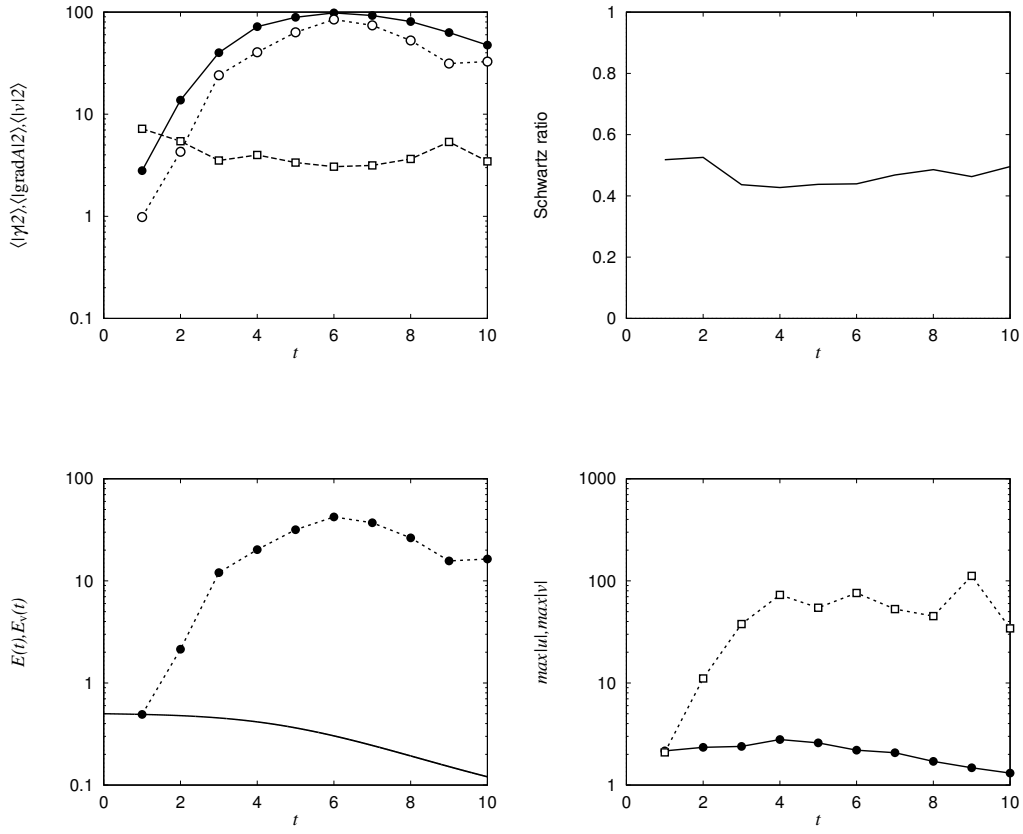
FIG. 9: Time evoultion of some quantities related to the composition $\boldsymbol{w} = (\nabla \boldsymbol{A})^T \boldsymbol{v}$, a(top-left): $\langle |\boldsymbol{w}|^2 \rangle$(solid circles), $\langle |\boldsymbol{v}|^2 \rangle$(open circles), $\langle |\nabla \boldsymbol{A}|^2 \rangle$(open circles). b(top-right): $r(t)$, c(bottom-left): $E(t)$(solid), $E_v(t)$(solid circles), and d(bottom-right): $\max |\boldsymbol{u}|$(solid circles), $\max |\boldsymbol{v}|$(open circles).

region is important, because a fall-off at their tail is necessary for accurate calculation of $\boldsymbol{C}$. From their time development we see that they are well-resolved, for the low and the intermediate Reynolds numbers.

By applying Cauchy-Schwarz inequality to (5) we have

$$\langle |\boldsymbol{w}| \rangle \leq \langle |\nabla \boldsymbol{A}|^2 \rangle^{1/2} \langle |\boldsymbol{v}|^2 \rangle^{1/2},$$

where the equality holds when

$$\frac{\partial \boldsymbol{A}}{\partial x_i} = \lambda \boldsymbol{v} \text{ for all } i, \text{ for some } \lambda.$$

It is of interest to check how the growth of $\boldsymbol{w}$ correlated with that of $\nabla \boldsymbol{A}$ and $\boldsymbol{v}$.

In Fig.9a the time evolution of $\langle |\boldsymbol{w}|^2 \rangle$, $\langle |\nabla \boldsymbol{A}|^2 \rangle$, $\langle |\boldsymbol{v}|^2 \rangle$ is shown together with the ratio for the case of turbulence. In Fig.9b, we plot the time evolution of

$$r(t) \equiv \frac{\langle |\boldsymbol{w}| \rangle}{\langle |\nabla \boldsymbol{A}|^2 \rangle^{1/2} \langle |\boldsymbol{v}|^2 \rangle^{1/2}}.$$

13
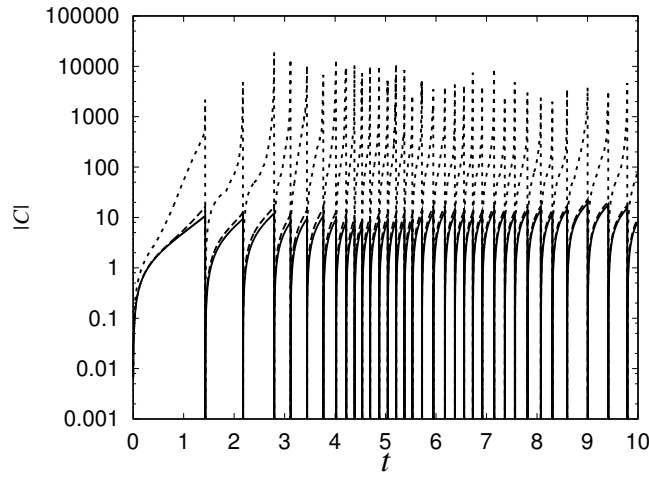
FIG. 10: Time evoultion of norms of $\boldsymbol{C}$, $L_1$-norm (solid), $L_2$-norm (dashed) and $L_\infty$-norm (dotted).

.

Roughly, the value of $r(t)$ is about 0.5, which means $\dfrac{\partial \boldsymbol{A}}{\partial x_i}$ is neither parallel nor perpendicular to $\boldsymbol{v}$ for all $i$, it fluctuates just around the mid-point in the admissible range $0 \le r(t) \le 1$. Because of frequent resetting, $\langle |\nabla \boldsymbol{A}|^2 \rangle \approx 3$ most of the time and consequently $\langle |\boldsymbol{v}|^2 \rangle$ tracks $\langle |\boldsymbol{w}|^2 \rangle$ fairly well.

In Fig.9c we show time development of $\max_{\boldsymbol{x}} |\boldsymbol{v}|$ and $\max_{\boldsymbol{x}} |\boldsymbol{u}|$. Also, we compare in Fig.9d time development of the total energy $E(t)$ with that of virtual velocity, that is, with

$$E_{\boldsymbol{v}}(t) = \frac{1}{2}\left\langle |\boldsymbol{v}|^2 \right\rangle.$$

Figure 9c shows that $|\boldsymbol{v}| \gg |\boldsymbol{u}|$. It should be noted that $\boldsymbol{v}$ does not grow at all in the case of totally inviscid case, where the virtual velocity $\boldsymbol{v}$ reduces to initial velocity (constant). It is the term $2\nu \boldsymbol{C} : \nabla \boldsymbol{v}$ in (7) which is responsible for the growth of $\boldsymbol{v}$. In (7), $|\boldsymbol{C}|$ becomes so large that its viscous term remains huge in spite of small value of $\nu$.

In Fig.10 we show the time development of several different norms of $\boldsymbol{C}$. It shows how rapidly $|\boldsymbol{C}|$ increases, particularly in its maximum value. Now we are in a position to characterize anomalous nature of turbulence by studying $\boldsymbol{C}$. Taking into account that $\boldsymbol{C}$ has a dimension of wavenumber we introduce the following definition. By connection anomaly we mean that for consecutive resetting times $[0, T]$ there exits $p \ge 1$ and a constant $A_p$ such that

$$\liminf_{\nu \to 0} \nu \int_0^T \left( \frac{1}{(2\pi)^3} \int |\boldsymbol{C}|^p d\boldsymbol{x} \right)^{2/p} \mathrm{d}t > A_p > 0. \tag{14}$$

14
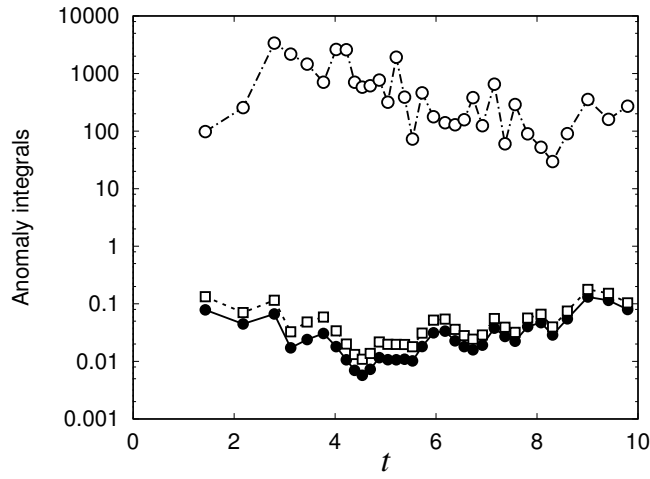
FIG. 11: Connection anomaly integrals, estimated with $L_1$-norm (solid circles), $L_2$-norm (open squares) and $L_\infty$-norm (open circles).
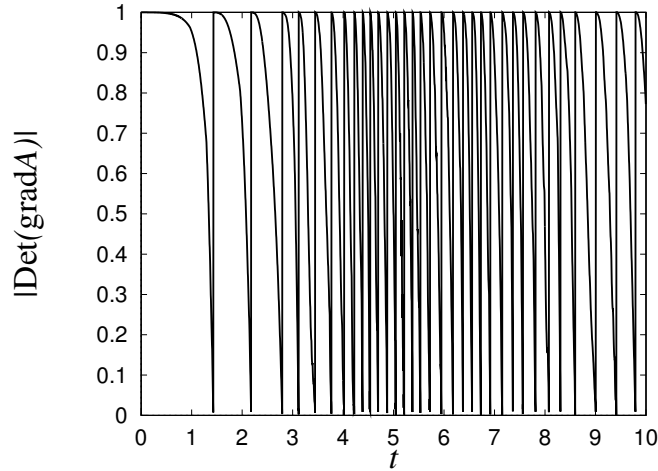


FIG. 12: Time evoultion of the determinant.

Here $A_p$ are positive constants which depend on the threshold $\epsilon$ for resetting and on the initial condition for velocity. This may be regarded as an analogue of dissipation anomaly in conventional theory.

In Fig.11 for we show the above non-dimensional integrals characterizing connection anomaly for each resetting time interval in the intermediate Reynolds number computation. It should be noted that the integrals evaluated with $L_1$, $L_2$ and $L_\infty$ norms appear to be bounded from below by positive constants of order $10^{-1}$, $10^{-1}$ and $10^2$ respectively.

In Fig.12 time development of $\text{Det}(\nabla \boldsymbol{A})$ is shown, which confirms that resetting is associated with rapid decrease in the magnitude of the determinant. At present, its form as a

15

function of $t$ is not known.

### C. The determinant $\mathrm{Det}(\nabla \boldsymbol{A})$

First, we study spatial locations of $\min_{\boldsymbol{x}}\mathrm{Det}(\nabla \boldsymbol{A})$. In principle, resettings can follow quickly each other in time, but could be brought about by distant events in space. There-fore, it is important to examine the spatial distribution of $\mathrm{Det}(\nabla \boldsymbol{A})$. Vortex reconnection processes in the case of turbulent flows may not be so prominent as compared with the ex-periment using orthogonally off-set vortex tubes. But it can occur in many places from time to time. Therefore, it is of interest to track the points of minimum $\mathrm{Det}(\nabla \boldsymbol{A})$ in time and see how it changes in time. We note that resettings do not necessarily imply singularities formation in some physical variables. Rather, the non-invertibility of the diffusive labels can monitor the phenomenon of vortex reconnection.

In Fig.13, the $x, y$ and $z$ components of a point with minimum $\mathrm{Det}(\nabla \boldsymbol{A})$ are plotted against time. For clarity, only a portion of time interval $5 \leq t \leq 7$ is shown, but its qualitative property is the same throughout the entire time interval of the computation. Roughly speaking, the position changes in time just like a piece-wise constant function, separated by resetting times designated by vertical dashed lines. Although there are some cases where the positions changes in wildly (e.g. in $5.72 \leq t \leq 5.95$), it should be noted that the position remains almost flat between successive resetting times.

In the case of the experiment using orthogonally off-set vortex tubes the position becomes stable (*i.e.* flat in the figure) only when the prominent reconnection process is taking place (see Fig.27 below).

Secondly, we study the probability distribution of $\mathrm{Det}(\nabla \boldsymbol{A})$. We have seen that the minimum value of the determinant becomes very small and hits zero under the time evolution of the Navier-Stokes equations. A natural question is how we can characterize spatial regions where the determinant is significantly smaller than 1. We examine how the determinant is distributed in space. In Fig.14 the probability distributions of the determinant are shown at several different times for the case of $\nu = 2.5 \times 10^{-3}$. At early stage $t = 1$, it is sharply localized around 1. After that it is spread a little for both smaller and larger determinants, but still strongly peaked at 1. The probability distribution at $t = 4$ looks exceptional because while it has a peak at 1, its tails cover a range $[0, 2]$. This shows that the determinants can

16

be not only small but also large compared with 1. Actually, there is a resetting shortly after at $t = 4.02$, the spread wings suggest that the resetting will take place soon. In a similar plot (not shown) exactly at a resetting time $t = 8.08$, there are widely spread wings over the range $[0, 2]$. The distribution of the determinant is highly localized at 1 for most of the time, it is broadly distributed only just before resettings.

Thirdly, it is of interest to examine how the regions with relatively small determinant $\text{Det}(\nabla \boldsymbol{A})$ look like and to see if they are related with vortex structure or not. In Fig. 15-19 the regions with small values of determinant is shown for the case of $\nu = 2.5 \times 10^{-3}$. by white symbols together with vorticity iso-surfaces in blue for $t = 1, 2, 4, 6$ and $t = 8.08$, which is just at a resetting. At the early stage $(t = 1)$ when there are vorticity layers, the regions with small determinants also take the form of layers. It should be noted that they are not very well correlated with each other spatially. Rather, the regions with small determinants lie between prominent vorticity layers. At $t = 2$ there are still vorticity layers, but the regions with small determinants appear to be better correlated with them than $t = 1$. At $t = 4$ some vorticity layers have rolled up into vorticity tubes. It is these vortex tubes which show a stronger correlation with the region with small determinants. After $t = 6$ (after the peak of the enstrophy) there are lots of vortex tubes and the small determinants are found surrounding these tubes. At $t = 8.08$ just at a resetting, the regions with small determinants collapse with vortex tubes almost perfectly.

We conclude that in the developed stage the regions with small determinants collapse with or surround the high-vorticity regions. This is consistent with the idea that resetting characterize reconnection of vortex tubes.


### D.   Probability distribution of connection

Now we turn our attention to another important quantity in the Eulerian-Lagrangian framework, that is, the connection matrix $\boldsymbol{C}$.

First, we show the probability distributions of connection matrix are plotted at several different times in Fig.20. Most of the time, the distribution has faster-than-exponential tails at large $\boldsymbol{C}$, such typical examples are shown for $t = 6, 7$. At times just before resetting, for example at $t = 4$ and 9 it decays more slowly, that is, the PDF shows a power-law behavior as seen in Fig.21.

Secondly, we show the joint probability distribution between connection and vorticity. Recalling that the connection matrix measures curvature of particle paths, we study how regions with large values of connection are correlated with those with high vorticity or with high rate-of-strain.

In Fig.22, the joint probability distributions between vorticity and strain are plotted. They are given here to show that they have a standard property, such as studied in [27], and to be compared with Fig.23. Here, plotting conventions are that contours of $\log_{10} P(\tilde{\boldsymbol{\omega}}, \tilde{\boldsymbol{S}})$ are shown with equidistant level increment =1, where $\tilde{\boldsymbol{\omega}} = \boldsymbol{\omega}/\sqrt{\langle |\boldsymbol{\omega}|^2 \rangle}$, etc.

In Fig.23, the joint probability distributions between the vorticity and the connection matrix are plotted. Most of the times, vorticity is well correlated with relatively lower amplitudes of connection but it has weaker correlations with higher values of connection. Just before the resetting (say, at $t = 4$), vorticity has an extremely strong correlation with lower values of connection. The tails of connection responsible for resetting is not well correlated vorticity. The joint probability distributions between rate-of-strain and connection have a similar trend as above is seen (figures omitted).

## V.   RECONNECTION EXPERIMENTS AT HIGH REYNOLDS NUMBER

In a previous report, a flow starting from two orthogonally offset vortex tubes was investigated in [5]. That initial condition of two orthogonally placed vortex tubes, which was originally introduced to study vortex reconnection in detail with conventional methods of analysis, see [28]. In that work we observed that frequent resetting takes place during the reconnection phase and that it ceases when two vortex tubes finish their reconnection process. We recall that the identification of the reconnection based on visual inspection agrees with systematic analysis based on the Euler-Lagrange formulation.

Here we examine a flow starting from the same initial condition but with larger Reynolds number, $R_\lambda \approx 100$ ( in the developed stage ) [30]. Our objective is, first of all, to see whether small scale excitation persists after the prominent reconnection phase. Apparently, this flow has not been examined at high Reynolds numbers previously. More specifically, we are interested in examining spatial locations of minimum $\text{Det}(\nabla \boldsymbol{A})$, and in checking connection anomaly holds true or not. The spatial resolutions for this initial condition are $N = 256$ and $N = 512$, see Table I.

18

In Fig.24 we show the time evolution of norms of displacement $E_{\boldsymbol{\ell}}(t)$ for $N = 256, \nu = 4 \times 10^{-3}$, with two different $\epsilon = 0.01,\ 0.001$. As before, we observe frequent resetting during the reconnection phase. More importantly, the frequent resetting apparently takes place independently of $\epsilon$.

In Fig.25, spatial location of min $\mathrm{Det}(\nabla \boldsymbol{A})$ together with iso-surfaces of high vorticity, vortex lines. The symbol denotes a location with minimum $\det(\nabla \boldsymbol{A})$, which is located between the two interacting tubes. The energy spectrum $E(k)$ at $t = 6$ shows a range $E(k) \propto k^{-5/3}$ in the $N = 512$ run (figure omitted).

We compare in Fig.26 norms of displacement $E_{\boldsymbol{\ell}}(t)$ for two different Reynolds numbers with the same $\epsilon$. For larger $R_\lambda$, the resetting occurs more frequently and the amplitude of displacement becomes smaller. It should be noted that in the $512^3$ run the frequent resetting continues from $t = 4$ *and onward*. Recall that $t = 4$ is the time when vortex resettings was observed to begin in the $256^3$ run. It is this time interval with frequent resettings that we find an inertial subrange compatible with Kolmogorov similarity. The non-dimensional integral associated with connection anomaly was also evaluated in this case in the sense that (14) holds (figure omitted).

In Fig.27, we show spatial locations of min $\mathrm{Det}(\nabla \boldsymbol{A})$. In the time interval $3.5 \leq t \leq 4.5$ the position shows a plateau at $x = \pi$, which is the center of the domain at which reconnection takes place. A similar behavior is also observed in $8.5 \leq t \leq 9.5$, which suggests that we have another reconnection in that period (confirmed by vorticity iso-surface plots). This shows that the Eulerian-Lagrangian formalism offers an objective method for vortex reconnection.


## VI. SUMMARY AND OUTLOOK

We have presented an Eulerian-Lagrangian analysis of turbulence using two different kinds of initial conditions; a decaying isotropic turbulence developed from a random initial conditions and orthogonally offset vortex tubes.

Quantities that appear in the Eulerian-Lagrangian formalism are analyzed numerically in some detail, including evolution of displacement, resetting processes, spectra of connection and virtual velocity. The connection matrix plays a key role in monitoring vortex reconnection in an objective fashion and in characterizing the singular perturbation nature,

19

"connection anomaly", of the vanishing viscosity limit of the Navier-Stokes equations. On the other hand, it is revealed by a series of visualizations that regions with small values of the determinant $\mathrm{Det}(\nabla \boldsymbol{A})$ are spatially correlated with vortex structures in turbulence. This indicates that resettings characterize small-scale excitations associated with vortex reconnection.

As we stressed in Section IV.C, resettings do not imply singularities in physical variables. In the case of orthogonally offset vortex tubes, we have confirmed that we have frequent resettings during they undergo reconnection. In the case of turbulence, however, the definion of vortex reconnection becomes ambiguous. So, care should be taken in the interpretation of resettings. What we have shown is that also in this case resettings do occur and that the small determinants are found to be near the vortex structures.

The present work shows that it is useful to characterize fully-developed turbulence on the basis of the Eulerian-Lagrangian formalism. It would be of interest to look for exact solutions of the Navier-Stokes equations which show resettings. It is also of interest to apply the method to a flow whose topological complexity increases in time. For example, studying the relationship between the number of stagnation points and that of resetting will be of interest. Numerical simulations at higher spatial resolutions at $1024^3$ are also worth pursuing.
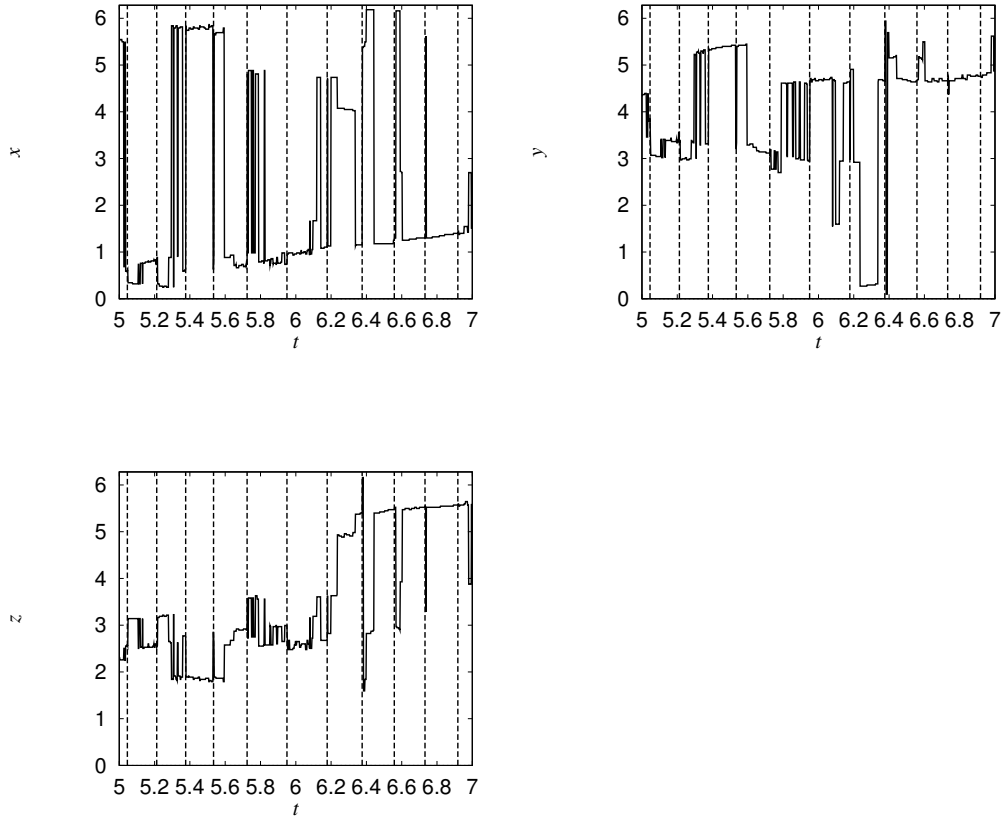
FIG. 13: Spatiail location of minDet($\nabla \boldsymbol{A}$) for the case of $\nu = 2.5 \times 10^{-3}$. The vertical lines denote each resetting.

|  | $\nu$ | $N$ | $\Delta t$ |
|---|---|---|---|
| turbulence 1 | $4 \times 10^{-3}$ | 256 | $2 \times 10^{-3}$ |
| turbulence 2 | $2.5 \times 10^{-3}$ | 256 | $2 \times 10^{-3}$ |
| turbulence 3 | $1.5 \times 10^{-3}$ | 512 | $2 \times 10^{-3}$ |
| vortex 1 | $4. \times 10^{-3}$ | 256 | $2.5 \times 10^{-3}$ |
| vortex 2 | $1.5 \times 10^{-3}$ | 512 | $2 \times 10^{-3}$ |

TABLE I: Numerical parameters

**ACKNOWLEDGMENTS**
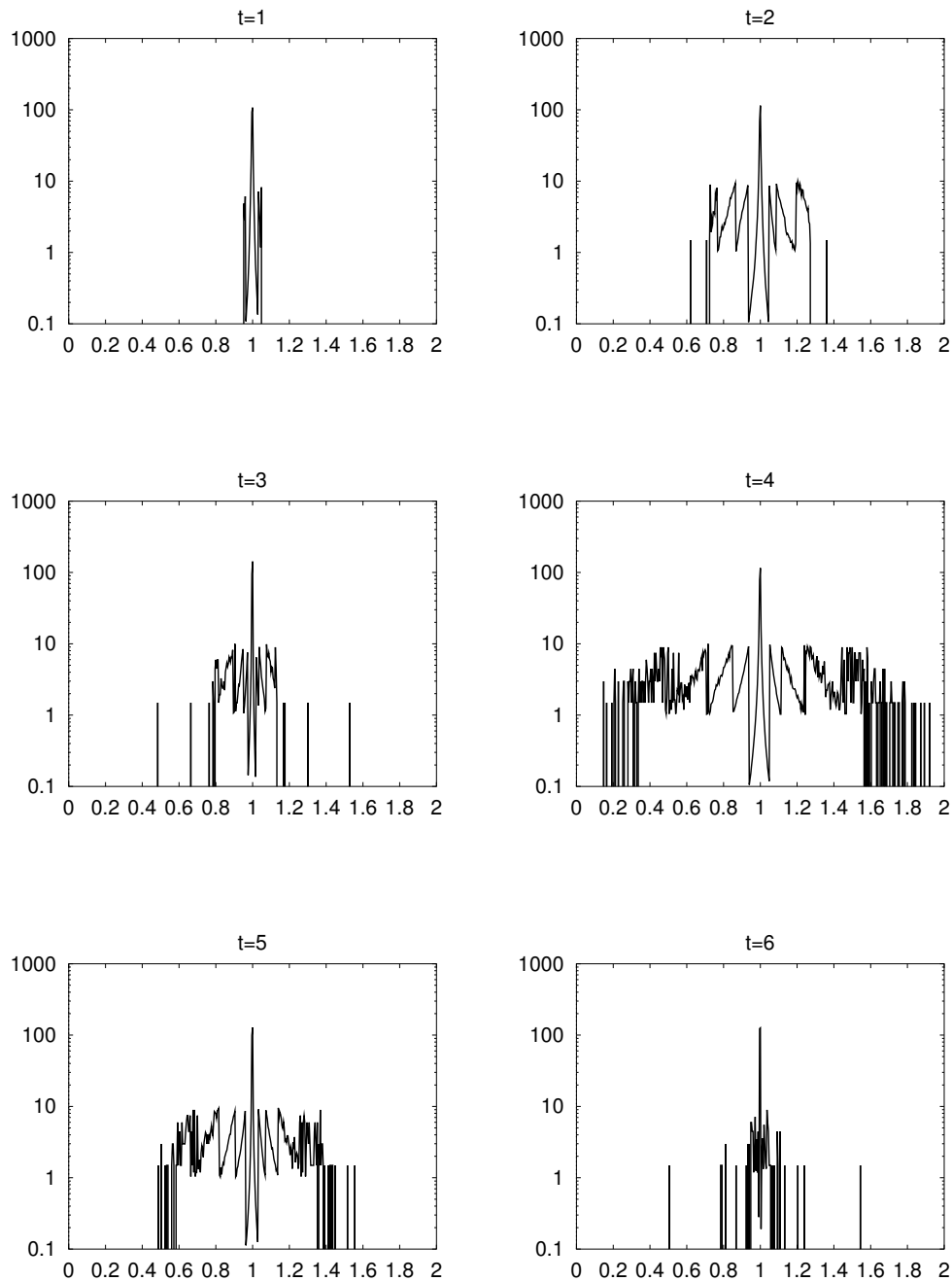
FIG. 14: The probability density function of the determinant.

FIG. 15: White symbols are placed in regions with $\det(\nabla \boldsymbol{A}) < 1.03 \min_{\boldsymbol{x}} \det(\nabla \boldsymbol{A}) \approx 0.980$ at $t = 1$. There are 76556 such points out of $256^3$. Iso-surfaces of vorticity are shown in blue $4 \langle |\boldsymbol{\omega}|^2 \rangle = 15.4$.

23
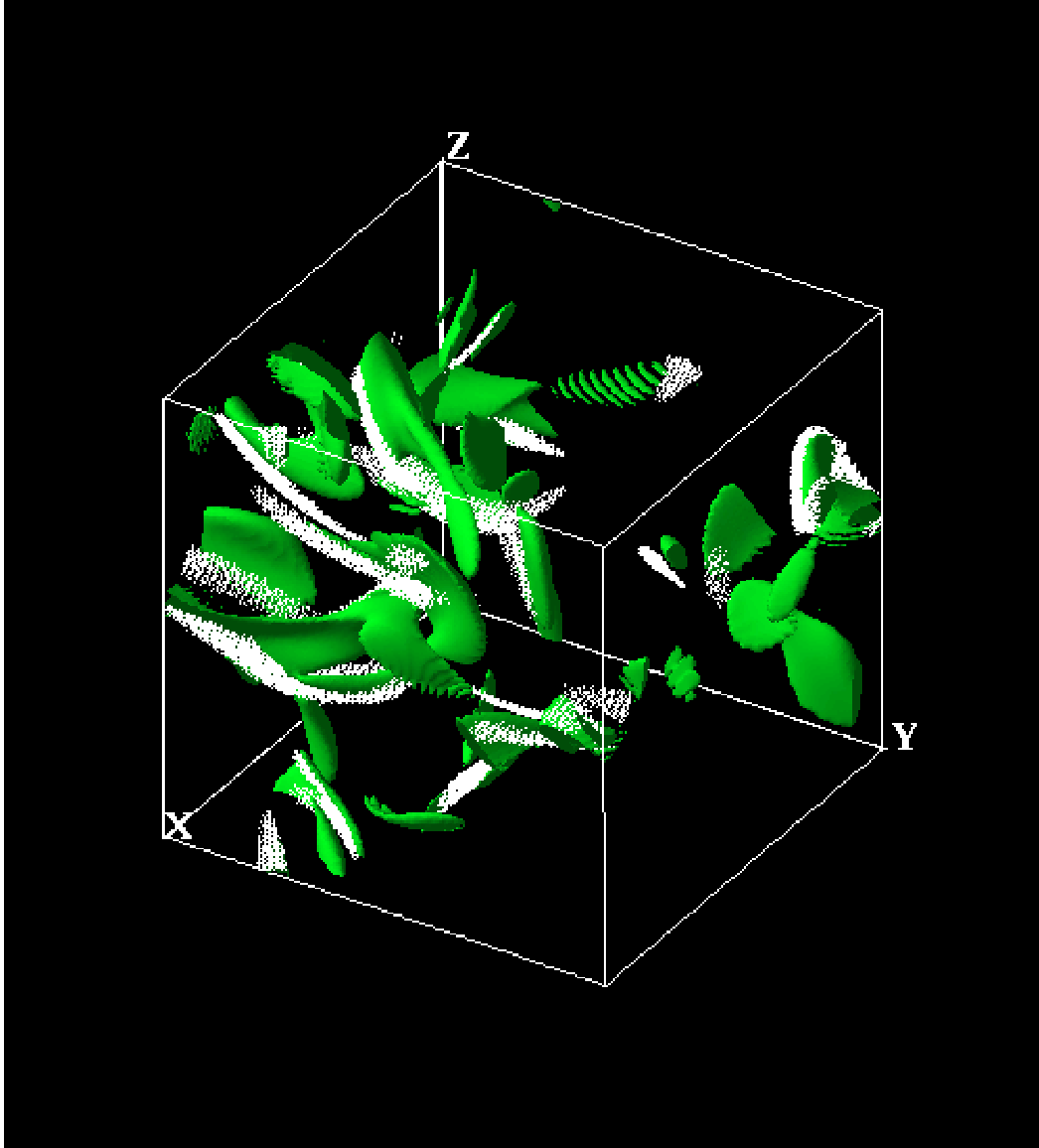
FIG. 16: White symbols are placed in regions with $\det(\nabla \boldsymbol{A}) < 1.3 \min_{\boldsymbol{x}} \det(\nabla \boldsymbol{A}) \approx 0.946$ at $t = 2$. There are 72696 such points out of $256^3$. Iso-surfaces of vorticity are shown in blue $4 \left\langle |\boldsymbol{\omega}|^2 \right\rangle = 36.25$.

24
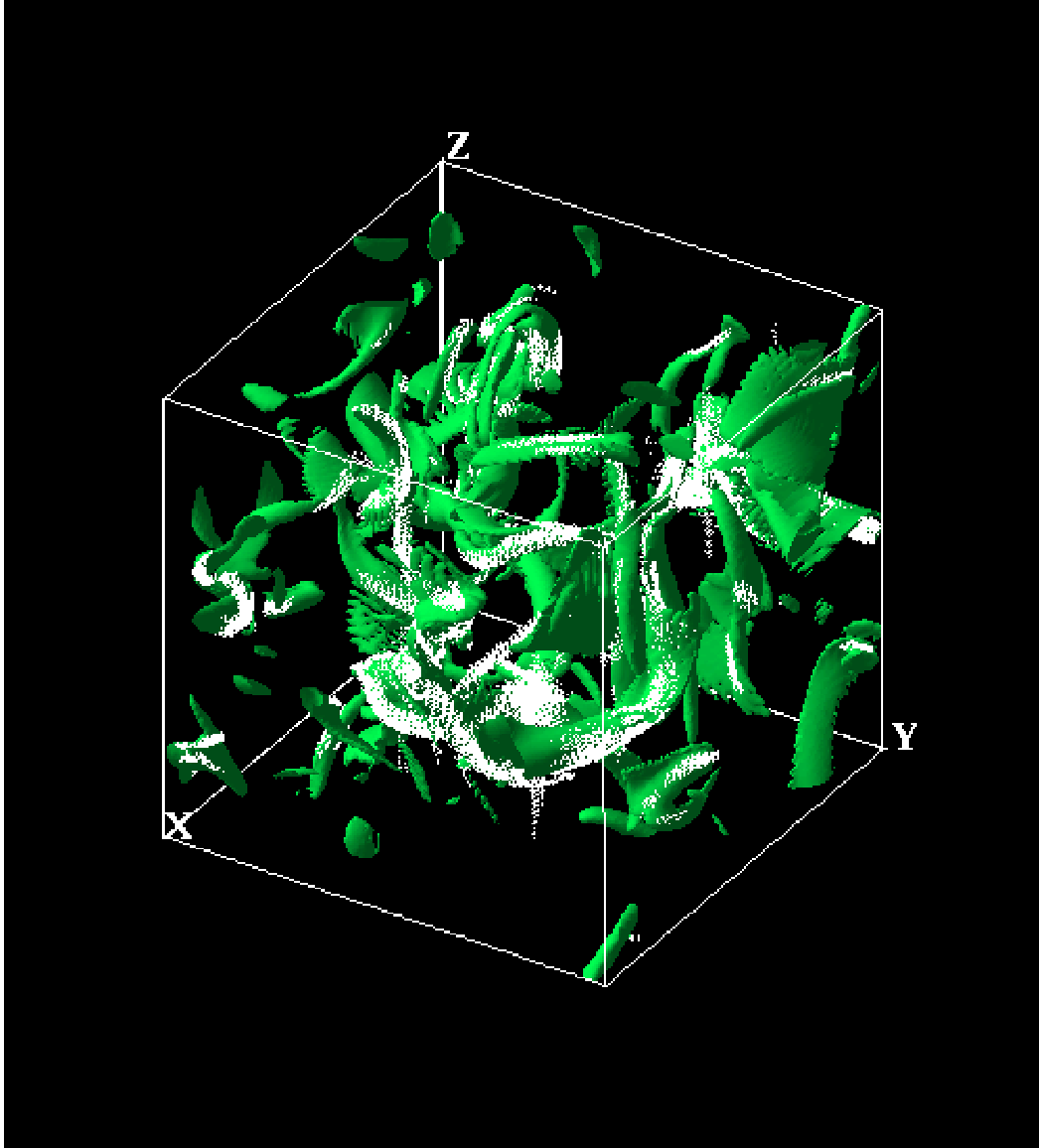
FIG. 17: White symbols are placed in regions with $\det(\nabla \boldsymbol{A}) < 11 \min_{\boldsymbol{x}} \det(\nabla \boldsymbol{A}) \approx 0.954$ at $t = 4$.
There are 93780 out of $256^3$. Iso-surfaces of vorticity are shown in blue $\langle |\boldsymbol{\omega}|^2 \rangle = 91.98$.
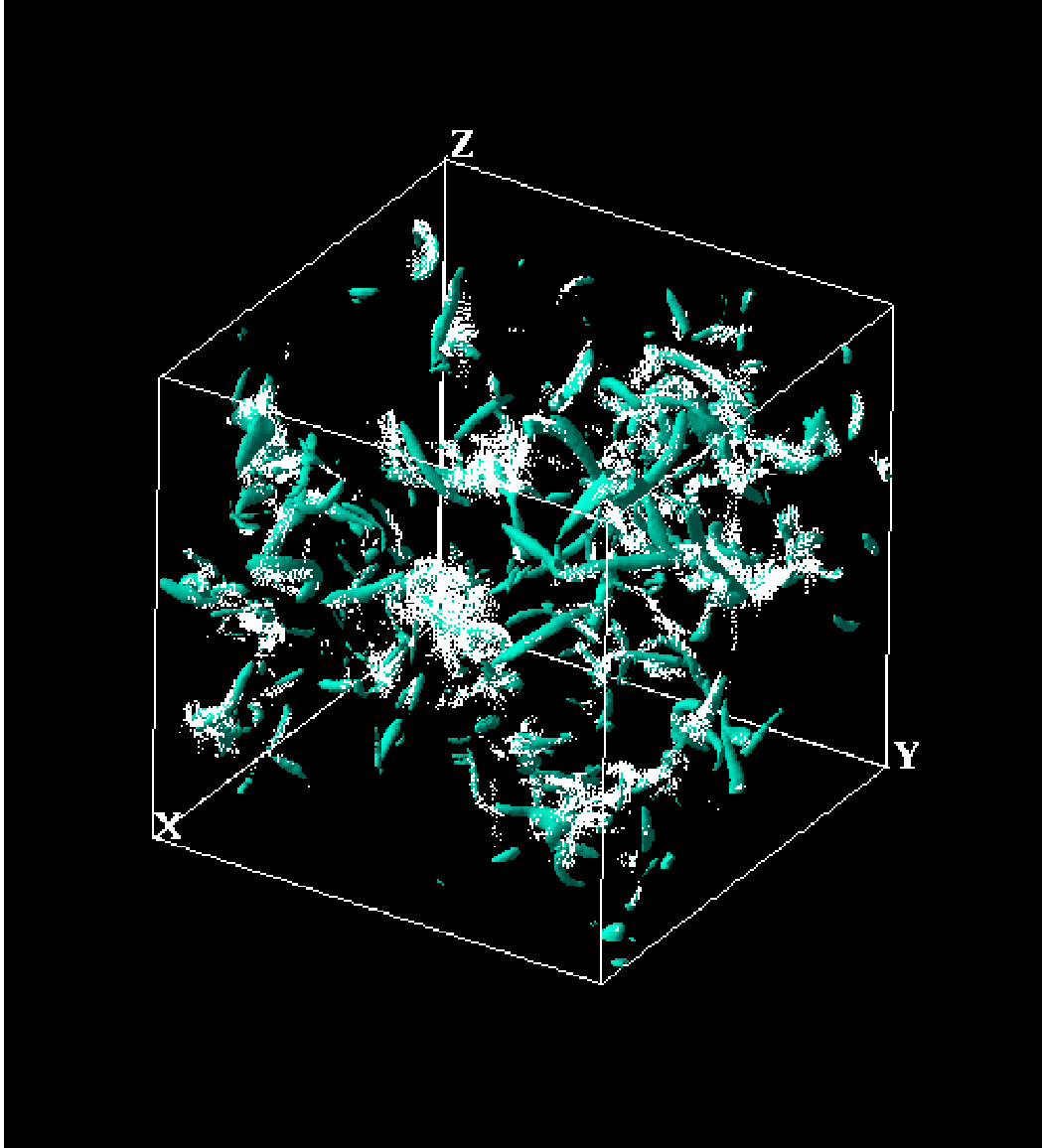
FIG. 18: White symbols are placed in regions with $\det(\nabla \boldsymbol{A}) < 1.045 \min_{\boldsymbol{x}} \det(\nabla \boldsymbol{A}) \approx 0.998$ at $t = 6$. There are 62838 out of $256^3$. Iso-surfaces of vorticity are shown in blue $10 \left\langle |\boldsymbol{\omega}|^2 \right\rangle = 243.0$.
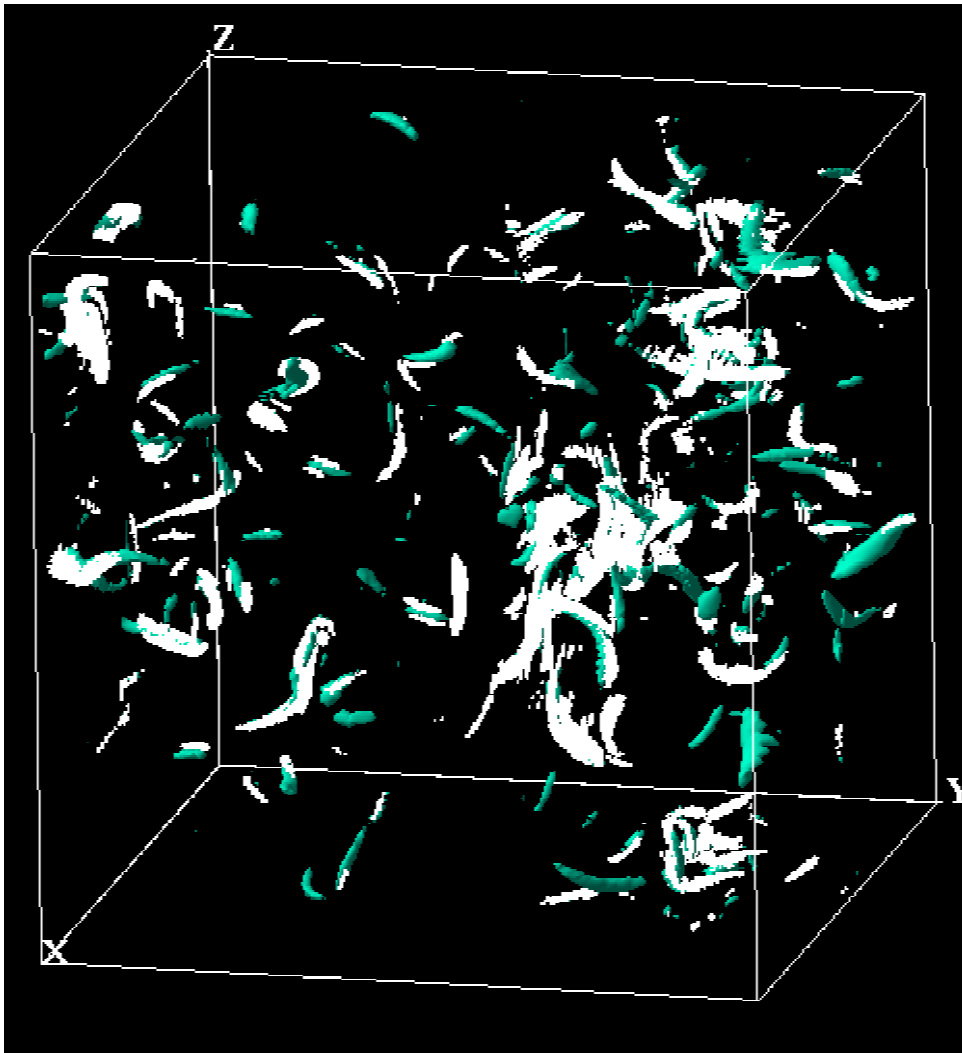
FIG. 19: White symbols are placed in regions with $\det(\nabla \boldsymbol{A}) < 110 \min_{\boldsymbol{x}} \det(\nabla \boldsymbol{A}) \approx 7.62 \times 10^{-3}$ at $t = 8.08$. There are 22943 such points out of $256^3$. Iso-surfaces of vorticity are shown in blue $|\boldsymbol{\omega}|^2 = 250$.

[1] P. Constantin, "Note on the loss of regularity of the 3D incompressible Euler and related equations," Commun. Math. Phys. **106**, 311(1986).

[2] P. Constantin, "An Eulerian-Lagrangian Approach to the Navier-Stokes Equations," Commun. Math. Phys. **216**, 663(2001).

[3] P. Constantin, "An Eulerian-Lagrangian Approach for incompressible fluids: local theory," J.
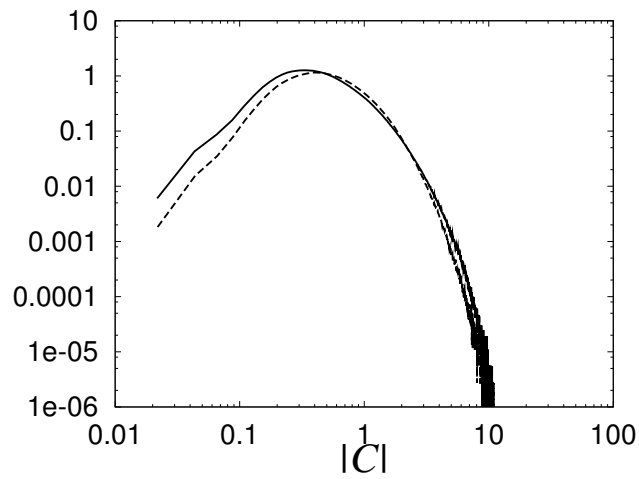
FIG. 20: The probability density function of connection at times $t = 6, 7$.
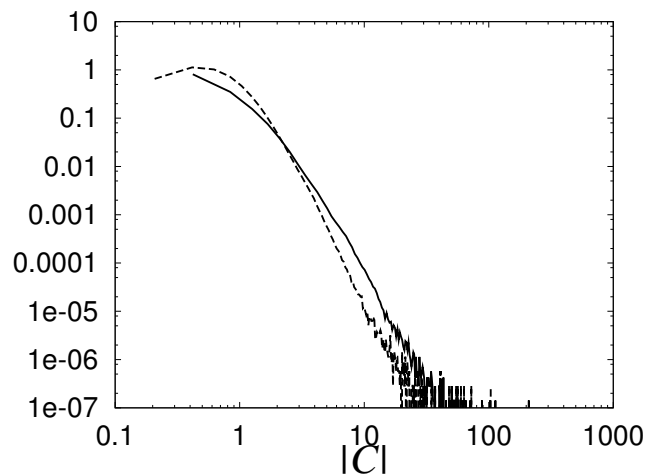


FIG. 21: The probability density function of connection at times $t = 4, 9$.

Amer. Math. Soc. **14**, 263(2001).

[4] P. Constantin, "Near identity transformations for the Navier-Stokes equations" in it Handbook of Mathematical Fluid Dynamics (ed. S. Friedlander and D. Serre). vol. 2, pp.117–141. Elsevier, 2003.

[5] K. Ohkitani and P. Constantin, "Numerical study of the Eulerian-Lagrangian formulation of the Navier-Stokes equations," Phys. Fluids **15**, 3251(2003).

[6] C. Cartes, C., M.Bustamante and M.E. Brachet, "Generalized Eulerian-Lagrangian description of Navier-Stokes dynamics," Phys. Fluids **19**, 077101(2007).

[7] P.H. Roberts, "A Hamiltonian theory for weakly interacting vortices," Mathematika **19**,
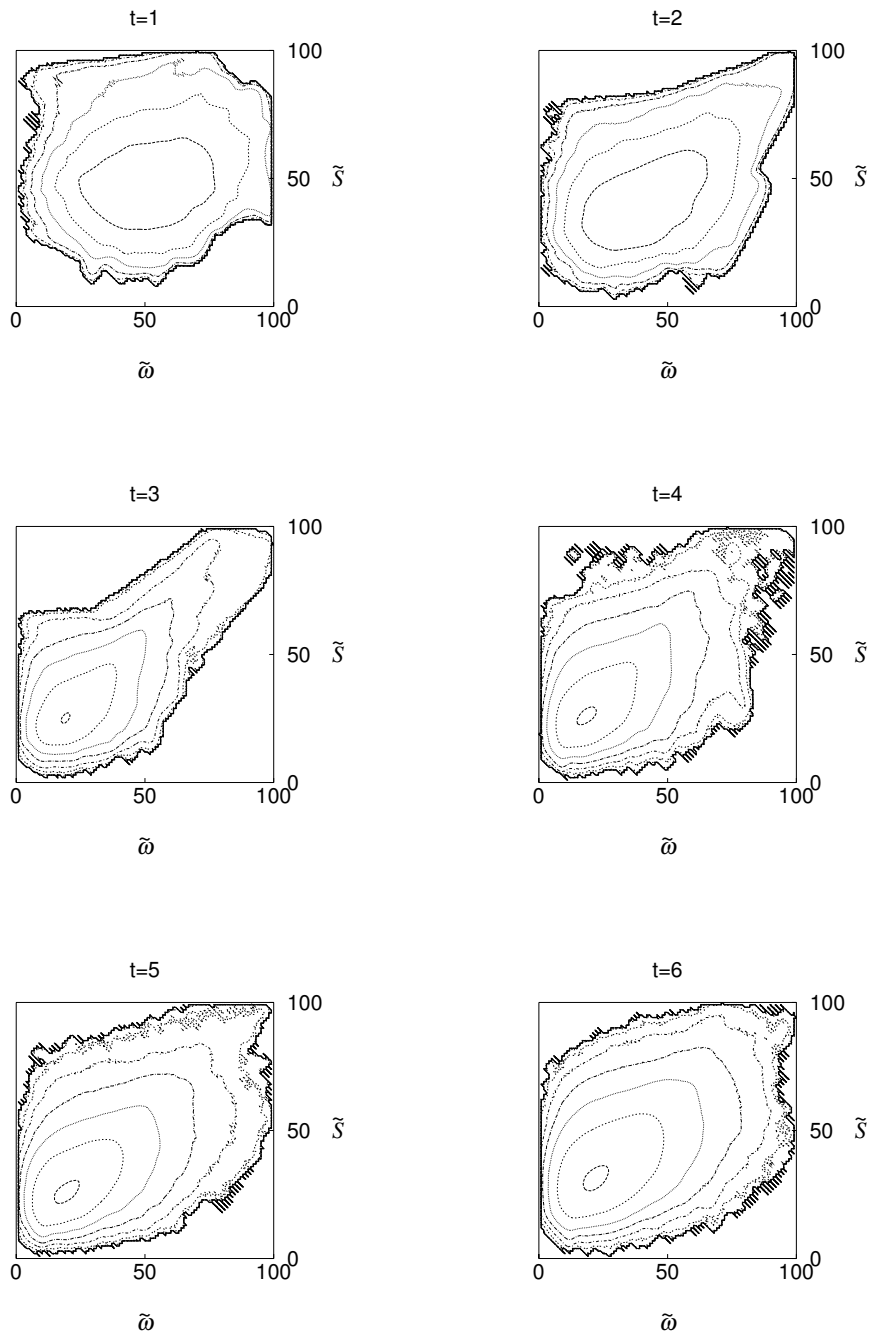
FIG. 22: The joint probability density function between vorticity and strain.
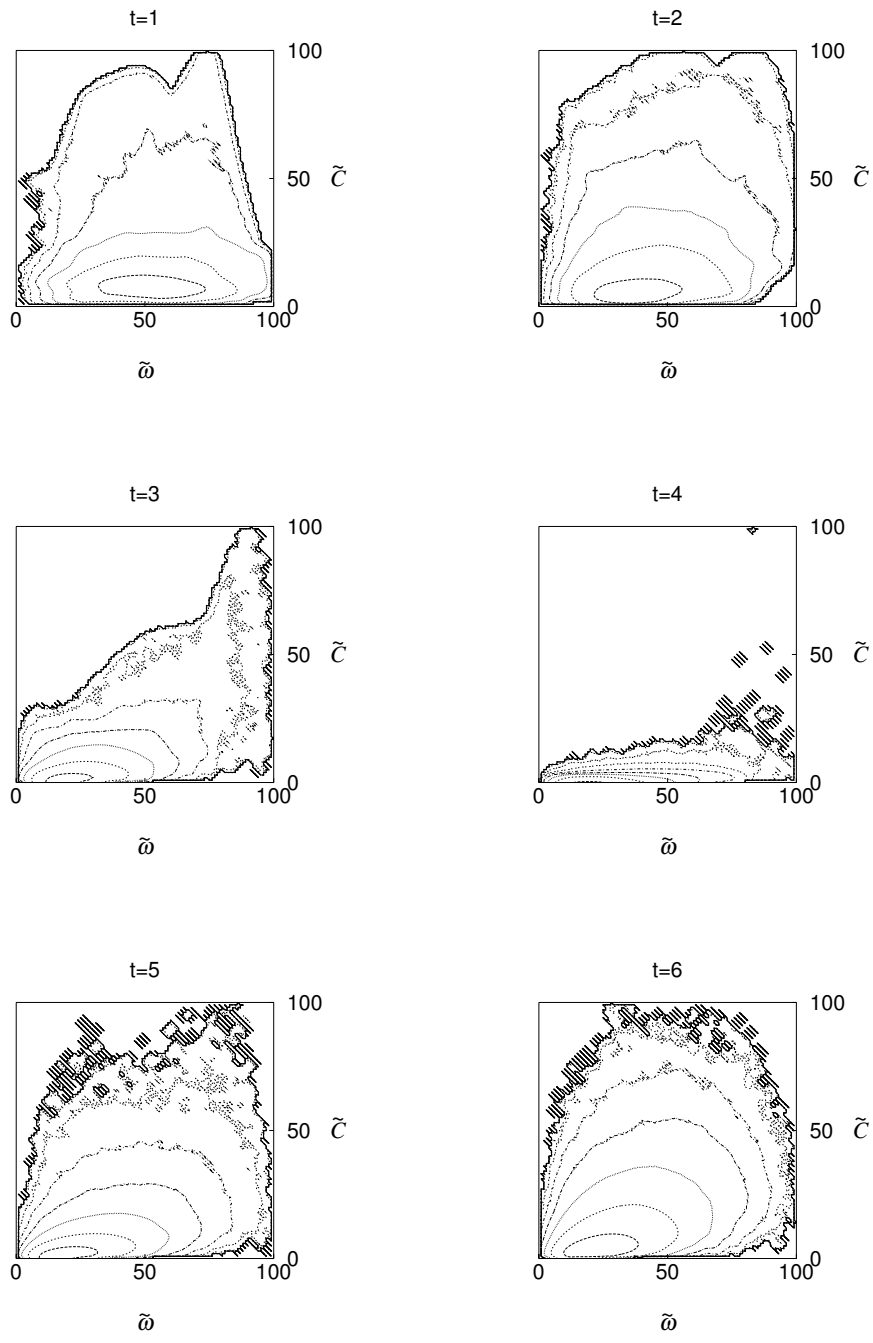
FIG. 23: The joint probability density function between vorticity and connection.
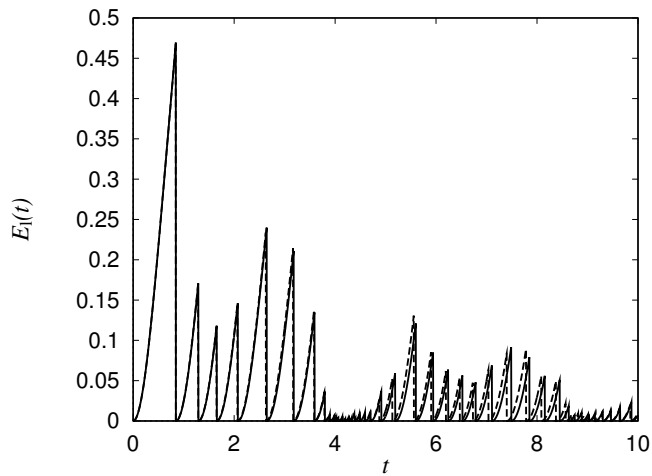
FIG. 24: Norms of displacement for with different values of threshholds: $\epsilon = 0.001$(solid), 0.01(dashed)

169(1972).

[8] T.B. Benjamin, T.B. "Impulse, flow force and variational principles," IMA J. Appl. Math. **32**, 3(1984).

[9] D.D Holm, "Lyapunov stability of ideal compressible and incompressible fluid equilibria in three dimensions," in *Hamiltonian structure and Lyapunov stability for ideal continuum dynamics, Sem. Math. Sup.* **100**, (University Montreal Press, Montreal, 1986) 125–208.

[10] Chefranov, S.G., "Dynamics of point vortex dipoles and spontaneous singularities in three-dimensional turbulent flows," Sov. Phys. JETP **66**, 85(1987).

[11] C. Anderson and C. Greengard, "The vortex ring merger at infinite Reynolds number," Comm. Pure Appl. Math. **42**, 1123(1989).

[12] V.I. Oseledets, "On a new way of writing the Navier-Stokes equation. The Hamiltonian formalism," Russ. Math. Surveys **44**, 210(1989).

[13] T.F. Buttke, "Velicity methods: Lagrangian numerical methods which preserve the Hamiltonian structure of incompressible flow," in *Vortex flows and related numerical methods,* NATO Adv. Sci. Inst. Ser. C Math. Phys. Sci. **395**, (ed. Eds. J.T. Beale, G. H. Cottet and S. Huberson, Kulwer, Norwell, 1993) 39.

[14] T. Buttke and A. Chorin, "Turbulence calculations in magnetization variables," Appl. Num. Math. **12**, 47(1993).

[15] S. Gama and U. Frisch, "Local helicity, a material invariant for the odd-dimensional incom-
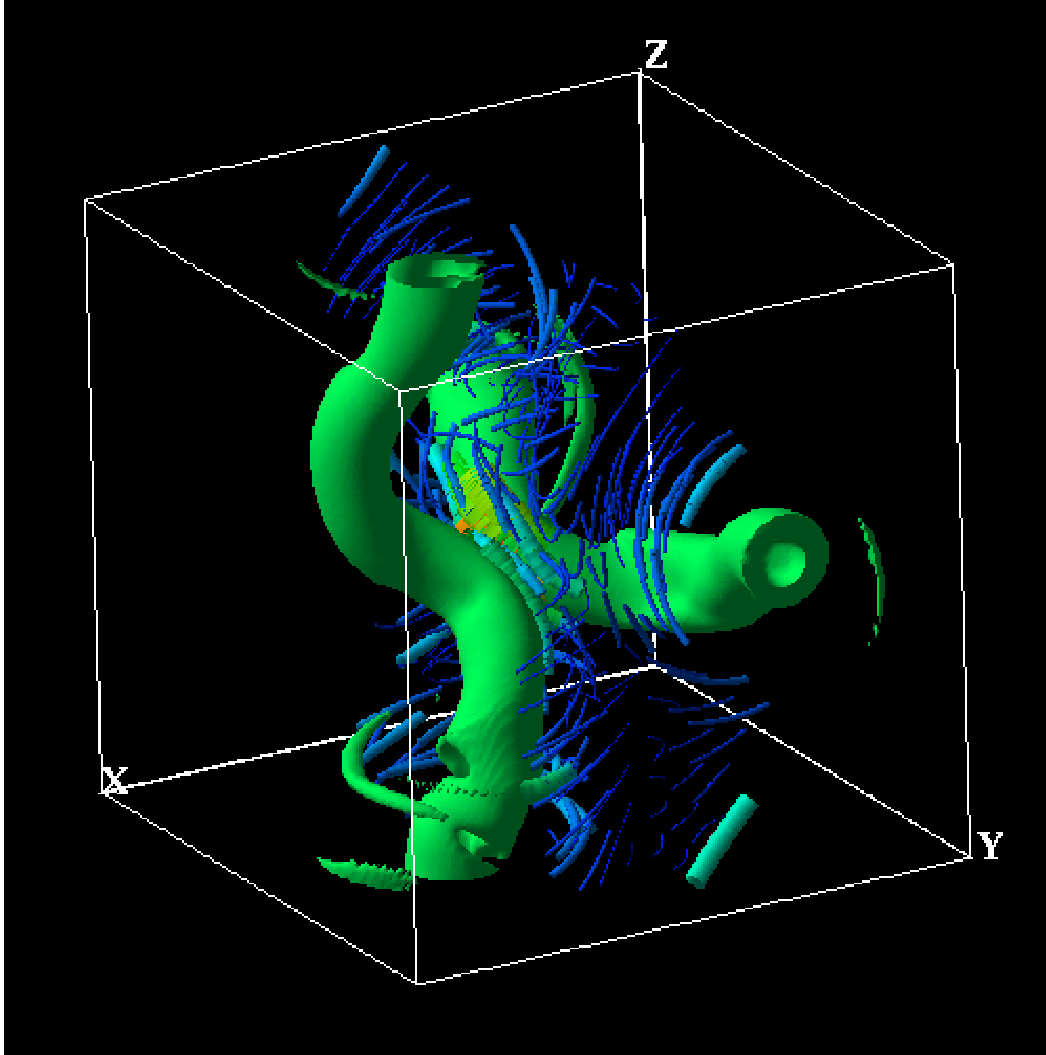
FIG. 25: Iso-surfaces of two vortex tubes at $t = 3.0$. The thin lines denote vortex lines in the interacting zone. A symbol (yellow, online) denotes a location of minimum $\det(\nabla \boldsymbol{A})$, which is just located between the two tubes.
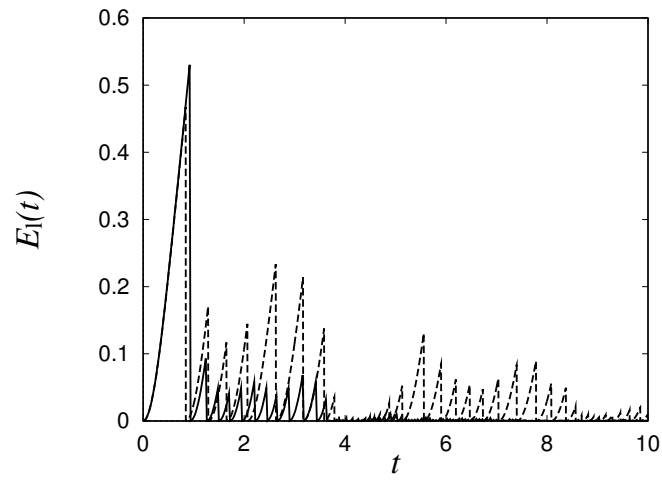
FIG. 26: Norms of displacement for $N = 256$, $\nu = 4 \times 10^{-3}$(dashed) and $N = 512, 1.5 \times 10^{-3}$(solid) with $\epsilon = 0.01$.
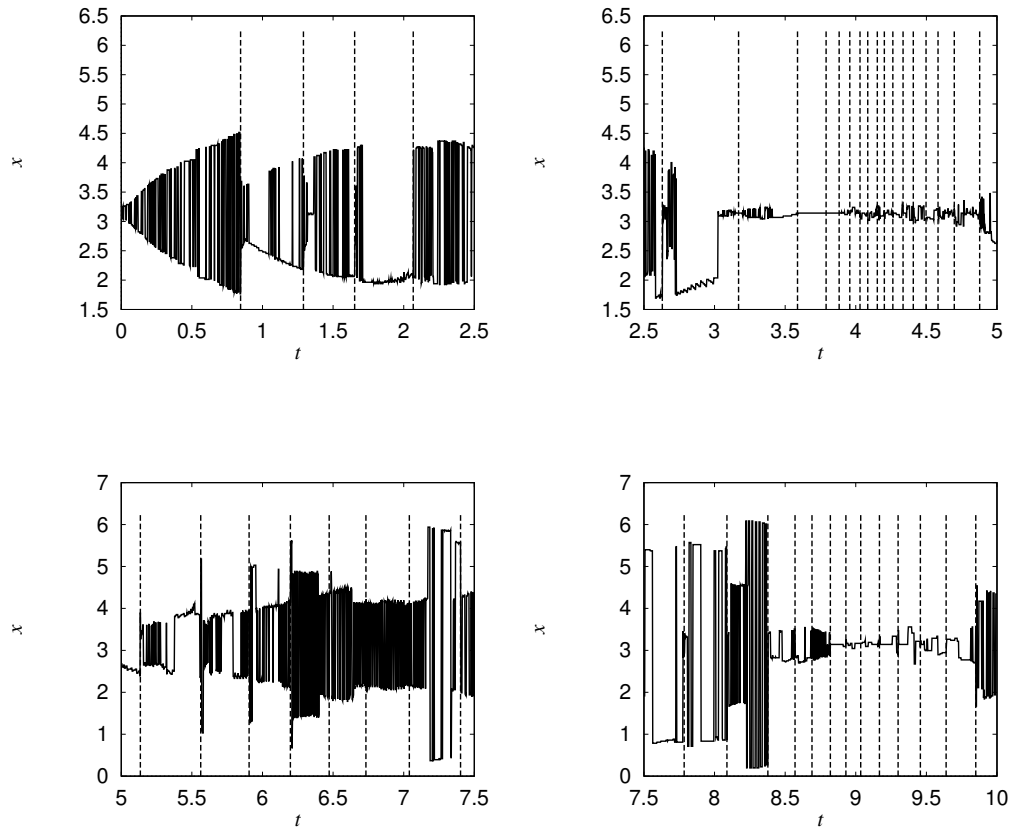


FIG. 27: Spatiail location of minDet($\nabla \boldsymbol{A}$) for the case of the reconnection experiments. The vertical lines denote each resetting.

pressible Euler equations," in *Solar and Planetary Dynamos, Publ. Newton Inst.* **1** (ed. M.R.E. Proctor *et al.*, Cambridge University Press, Cambridge, 1993), 115–119.

[16] A.J. Chorin, A.J., "Vortex phase transitions in $2\frac{1}{2}$ dimensions," J. Stat. Phys. **76**, 835(1994).

[17] J.R. Herring, R.M. Kerr and R. Rotunno, "Ertel's potential vorticity in unstratified turbulence," J. Atmos. Sci. **51**, 35(1994).

[18] J.H. Maddocks and R.L. Pego, "An unconstrained Hamiltonian formulation for incompressible fluid flows," Commun. Math. Phys. **170**, 207(1995).

[19] D. Summers and A. Chorin, "Numerical vorticity creation based on impulse conservation," Proc. Nat. Acad. Sci. U.S.A. **93**, 1881(1996).

[20] W. E and J.-G. Liu, "Finite difference schemes for incompressible flows in the velocity-impulse density formulation," J. Comput. Phys. **130**, 67(1997).

[21] G.A. Kuz'min, "Vortex momentum density and invariants of the hydrodynamic equations of superfluidity and superconductivity," Low Temp. Phys. **25**, 1(1999).

[22] G. Russo and P Smereka, "Impulse formulation of the Euler equations: General properties and numerical methods," J. Fluid Mech. **391**, 189(1999).

[23] D.M. Summers, "On the formation of vortices at a solid boundary," Proc. Roy. Soc. Lond. A, **456**, 1183(2000).

[24] D.M. Summers, "Towards an impulse-based Lagrangian model of boundary layer turbulence," Physica D **154**, 287(2001).

[25] W. E and J.-G. Liu, "Gauge method for incompressible flows," Commun. Math. Sci. **1**, 317(2003).

[26] G.A. Kuz'min, "Ideal incompressible hydrodynamics of the vortex momentum density," Phys. Lett. **96**A, 88(1983).

[27] J. Jimenez, A.A. Wray, P.G. Saffman and R.S. Rogallo, "The structure of intense vorticity in isotropic turbulence," J. Fluid Mech. **255**, 65(1993).

[28] O.N. Boratav, R.B. Pelz and N.J. Zabusky, "Reconnection in orthogonally interacting vortex tubes: Direct numerical simulations and quantifications," Phys. Fluids A **4**, 581(1992).

[29] Under the choice of another gauge, the first term on the RHS of (12) may be dropped without changing physics.

[30] Note that in [28], super-viscosity was used, so direct evaluation of $R_\lambda$ is not possible. Here we use usual Newtonian viscosity.